Tunable all-optical System for time-to-frequency mapping by parabolic cross-phase modulation in the spectral fraunhofer regime

Youcef Driouche, Badr-Eddine Benkelfat

IEEE Access
Multidisciplinary | Rapid Review | Open Access Journal

IEEE PHOTONICS SOCIETY SECTION

Received 4 September 2023, accepted 15 September 2023, date of publication 20 September 2023,
date of current version 28 September 2023.

Digital Object Identifier 10.1109/ACCESS.2023.3317517

RESEARCH ARTICLE

Tunable All-Optical System for Time-to-Frequency Mapping by Parabolic Cross-Phase Modulation in the Spectral Fraunhofer Regime

YOUCEF DRIOUCHE AND BADR-EDDINE BENKELFAT, (Senior Member, IEEE)
SAMOVAR Laboratory, Télécom SudParis, Institut Polytechnique de Paris, 91120 Palaiseau, France
Corresponding author: Youcef Driouche (youcef_driouche@telecom-sudparis.eu)

ABSTRACT According to the new condition of the pump peak power, we report a developed approach to achieve time-frequency mapping (TFM) in the spectral Fraunhofer regime by a single all-optical time lens using parabolic cross-phase modulation (XPM). The condition is obtained by combining the far-field spectral Fraunhofer regime with the ability of parabolic pump pulses to induce a pure quadratic phase modulation. The derived condition allows the tunability of the mapping by different strategies when probe pulses with different durations are targeted. For design requirements, we show the complete family of bright and dark parabolic pump pulses, which can be implemented depending on the shape of the probe. In order to overcome the limits of the far-field TFM, we demonstrate as a solution the so-called near-field TFM for narrowband mapping. We also discuss potential applications in a variety of fields to provide more insight into the developed approach.

INDEX TERMS Spectral Fraunhofer regime, cross-phase modulation, time-to-frequency mapping.

I. INTRODUCTION

Time-to-frequency mapping (TFM) is the conversion of an optical pulse envelope from the time domain into the frequency domain. Several techniques have been reported in order to realize the TFM; for instance, a reconfigurable optical arbitrary waveform generator has been demonstrated to synthesize an arbitrary broadband optical spectrum starting from a CW laser via a recirculating frequency shifting loop (FSL). The first step consists of modulating the CW temporally in amplitude and phase with an input electrical signal having a low-bandwidth. The resulting signal is circulated for multiple rounds through the FSL, leading to a modification in the amplitude and phase of the optical spectrum proportionally to the temporal shape of the modulation input signal, and as a result, the TFM is achieved [1]. Further, an accelerating grating can induce distinct phase-matching conditions during the nonlinear interaction at different times. Spatiotemporal quasi-phase-matching with specific accelerating modulations was proposed to control the spectral and temporal profiles of high-harmonic generation [2] and for TFM of optical pulses [3]. Furthermore, nonlinear pulse shaping based on self-phase modulation (SPM) can also be implemented by controlling line-by-line the amplitude and phase of the input pulse by using a spatial light modulator followed by a highly nonlinear fiber (HNLF). The results show that TFM can be precisely realized by obtaining a purely quadratic temporal phase in the HNLF, and the scheme is suitable for any arbitrary input temporal profile [4].

In addition to these techniques, high-fidelity mapping has been achieved based on the spectral Fraunhofer regime, where the optical pulse envelope is spectrally modified by the action of a single time lens (TL). Under specific conditions, the temporal envelope of the optical pulse can be mapped into the frequency domain with full energy preservation [5]. The TL process, which induces a temporal quadratic phase

The associate editor coordinating the review of this manuscript and approving it for publication was Liam Barry.

modulation, can be employed using an electro-optical phase modulator (EO-PM) driven by a sinusoidal radio frequency signal [6]. Unfortunately, EO-PM has limited performance, such as the electrical modulation bandwidth that significantly limits the processing speed and the ability to obtain a purely quadratic phase.

Optical pulses with parabolic temporal intensity profiles have gotten much interest for a variety of applications, starting from high-power ultrashort pulse generation to optical nonlinear signal processing [7], [8], [9], [10]. These parabolic pump pulses can be generated with different durations ranging from the sub-picosecond to a few tens of picoseconds by linear or nonlinear pulse shaping techniques [11], [12], [13] and birefringent filters [14], [15]. Since it is well known that parabolic XPM can induce quadratic phase modulation on a probe pulse [16], many works based on XPM have been done in the last three decades in order to eliminate optical pulse degradation [17], [18], [19], spectral compression [20], and real-time temporal measurement of femtosecond pulses [21]. Most of these works require the presence of a dispersive medium to create a dispersion-XPM configuration arranged in an appropriate balance.

In this paper, based on parabolic XPM, we drive a new condition of the pump peak power to achieve TFM in the far-field spectral Fraunhofer regime by a single all-optical time lens. This condition combines the far-field spectral Fraunhofer regime and the XPM ability to generate quadratic phase modulation. This combination allows us to link the pump peak power with the linear chirp coefficient and the prerequisites of the XPM process. Unlike the previous techniques presented, our proposal relies on the fact that XPM offers an intrinsic physical property for high temporal resolution, full energy conservation due to the nonlinear phase-only modulation, and a single-time-lens. Additionally, we investigated the system's tunability relying on two suggested strategies, which give options for the proposed system's implementation. Moreover, we introduce a complete family of pump pulses for design purposes, depending on the symmetric and non-symmetric target probe profiles. A solution based on the near-field TFM regime was proposed to overcome the limitations of the far-field TFM regime in narrowband mapping. Finally, a discussion has been provided to significantly increase the scope of the approach towards potential application.

II. THEORY

Before centering our attention on the new derived condition and for more self-content, we briefly review the spectral Fraunhofer regime through a time lens. Let $a_{in}(t)$ and $a_{out}(t)$ be the temporal envelopes of the input and output pulses from a time lens action, respectively. The relationship between $a_{in}(t)$ and $a_{out}(t)$ is given by a simple product as $a_{in}(t)$. $g(t) = a_{out}(t)$, where $g(t)$ is the function of a time-lens operator. The function $g(t)$ is known as a temporal quadratic phase modulator of the form,

$$g(t) = \exp\left[j\varphi(t)\right] = \exp\left(j\frac{\varphi_t}{2}t^2\right) \tag{1}$$

where $\varphi_t = [\partial^2\varphi(t)/\partial t^2]_{t=0}$, is the linear chirp coefficient of the time-lens process. The Fourier transform of the function $g(t)$ is given as $G(\omega) = \exp[-j(1/2\varphi_t)\omega^2]$, where ω is the angular frequency. We can write the relationship between the spectrum of the input pulse $A_{in}(\omega)$ and output pulse $A_{out}(\omega)$ by a convolution product as,

$$\begin{aligned} A_{out}(\omega) &= A_{in}(\omega) * G(\omega) \\ &= \int_{\Delta\omega_{in}} A_{in}(\sigma)\exp\left(-\frac{j}{2\varphi_t}(\omega-\sigma)^2\right)d\sigma \\ &= \exp\left(-\frac{j}{2\varphi_t}\omega^2\right)\int_{\Delta\omega_{in}} A_{in}(\sigma)\exp\left(-\frac{j}{2\varphi_t}\sigma^2\right) \\ &\quad\times\exp\left(\frac{j}{\varphi_t}\omega\sigma\right)d\sigma \end{aligned} \tag{2}$$

where σ is the integration variable, and $\Delta\omega_{in}$ is the full spectral width of $A_{in}(\omega)$. If $A_{in}(\omega)$ is confined to a small bandwidth $\Delta\omega_{in}$, and if the linear chirp coefficient is sufficiently large,

$$|\varphi_t| \gg \frac{\Delta\omega_{in}^2}{8\pi} \tag{3}$$

then, the phase term $\exp[-j(1/2\varphi_t)\sigma^2]$ is considered negligible. We could say that the inequality (3) is the far-field spectral Fraunhofer regime, and it is valid if the linear chirp coefficient φ_t is much greater than the square of the input pulse bandwidth $\Delta\omega_{in}$. Therefore, Eq. (2) may be approximated as,

$$\begin{aligned} A_{out}(\omega) &= \exp\left(-\frac{j}{2\varphi_t}\omega^2\right)\int_{\Delta\omega_{in}} A_{in}(\sigma)\exp\left(\frac{j}{\varphi_t}\omega\sigma\right)d\sigma \\ &= \exp\left(-\frac{j}{2\varphi_t}\omega^2\right)\left\{\mathcal{F}^{-1}[A_{in}(\omega)]\right\}_{t=\omega/\varphi_t} \end{aligned} \tag{4}$$

where $\mathcal{F}^{-1}$ denotes the inverse Fourier transform. Hence, under inequality (3), the input temporal pulse envelope $a_{in}(t)$ is mapped to the spectral domain evaluated at the instant $t = \omega/\varphi_t$. Since the output spectrum is associated with an additional phase term, $\exp[-j(1/2\varphi_t)\omega^2]$, the TFM is performed only by recovering the magnitude of the inverse Fourier transform. In the following, we demonstrate that the required time-lens process to induce the far-field TFM can be obtained using XPM on a target optical pulse as a probe signal, including symmetric and non-symmetric intensity profiles, with a parabolic optical pulse as a pump signal. This single all-optical time lens is achieved based on the exact value of the pump peak power from the following derivative condition.

The schematic in Fig. 1 depicts our proposed approach. In our scheme, the parabolic pump pulse co-propagates with the probe pulse in a highly nonlinear fiber (HNLF). We suppose that the pump and probe signals are synchronized at the input of the HNLF and have the same polarization state. Moreover, to avoid spectra overlap, the temporal walk-off effect, and dispersion, we assume that the wavelengths of the pump λ_{Pump} and the probe λ_{Probe} are symmetric and

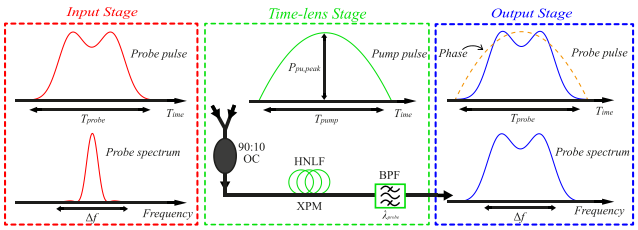

FIGURE 1. Schematic diagram of the proposed XPM-based far-field TFM approach using a parabolic pump pulse. OC: Optical Coupler, HNLF: Highly Nonlinear optical Fiber, BPF: Bandpass Filter.

close enough to the HNLF's zero-dispersion wavelength. Under these conditions, the probe pulse experiences a nonlinear phase modulation that can be mathematically described as [22],

$$\phi_{XPM} = 2\gamma L_{eff} P_{pump}(t) \tag{5}$$

where γ is the nonlinear coefficient at the probe wavelength ($\gamma = n_2 k_0 / A_{eff}$, where n_2 is the nonlinear refractive index, $k_0 = 2\pi/\lambda_{Probe}$ is the wavenumber, and A_{eff} is the effective mode area), $P_{pump}(t)$ is the pump's temporal intensity envelope at the HNLF input, and L_{eff} is the effective length of the fiber given as,

$$L_{eff} = \frac{1 - \exp(-\alpha L_{HNLF})}{\alpha} \tag{6}$$

where α is the loss coefficient defined as $\alpha \approx \alpha_{\mathrm{dB/km}}/4.34$, $\alpha_{\mathrm{dB/km}}$ is the attenuation coefficient in log scale, and L_{HNLF} is the physical length of the HNLF). Under the given circumstances, XPM will not affect the temporal intensity envelope of the probe; however, it will have an effect on the power spectral density. The maximum nonlinear induced phase can be expressed as $\phi_{XPM,\max} = 2\gamma\ L_{eff}\ P_{Pu\_Peak}$, where P_{Pu_Peak} is the pump peak power. After the HNLF, the pump is filtered-out by a bandpass filter centered at the probe wavelength. On the other hand, when $t = T_{pump}/2$, the maximum nonlinear induced phase is obtained, where T_{pump} is the total temporal width of the pump pulse. By substituting in the phase of Eq. (1), we find the maximum quadratic phase modulation of the time-lens process as,

$$\varphi_{\max} = \frac{\varphi_t}{2}\left(\frac{T_{pump}}{2}\right)^2 \tag{7}$$

Based on the expression of the maximum nonlinear induced phase, Eq. (7) can be expressed as $2\gamma\ L_{eff}\ P_{Pu\_Peak} = (\varphi_t/2)(T_{pump}/2)^2$. Thereby, the condition of the pump peak power to achieve TFM in the far-field spectral Fraunhofer regime is,

$$P_{pu\_peak} = \frac{\varphi_t T_{pump}^2}{16\gamma L_{eff}} \tag{8}$$

where φ_t must satisfy the inequality (3). Eq. (8) implies that different values of the pump peak power could be attained depending on the choice of the appropriate T_{pump} that must be greater than or equal to the total time width of the input probe T_{probe}, the HNLF parameters, and the linear chirp coefficient φ_t, which is completely independent of the system. Also, condition (8) allows the system to be tunable for mapping any input pulse profile having different durations by controlling P_{Pu_Peak} or T_{pump}.

III. RESULTS AND DISCUSSIONS

A. FAR-FIELD TIME-TO-FREQUENCY MAPPING

In this section, we carried out a numerical proof of concept of the parabolic XPM implementation for far-field TFM relying on the derived condition (8). We have tested different input pulses with symmetric and non-symmetric intensity profiles. First, an unchirped third-order super-Gaussian profile (similar to a flattop pulse) with a total temporal width of $T_{probe} \approx 50$ ps was assumed as the probe pulse. The probe is fully covered by taking into account the small residual amplitudes at the edges of the pulse. The total bandwidth of this probe pulse was $\approx 2\pi \times 213.33$ GHz (zero-to-zero full width). Based on the inequality (3), the corresponding linear chirp coefficient must satisfy $\varphi_t \gg \Delta\omega_{in}^2/8\pi = 7.14 \times 10^4$ rad GHz^2. In most cases, the quantity of φ_t should be a few times (~3-4) more than the inequality's right-hand side term. For simplicity, we introduce a new parameter n to set a fixed value of φ_t so that the inequality (3) becomes $\varphi_t = n \times \Delta\omega_{\mathrm{in}}^2/8\pi$. By putting $n = 4$, we found $\varphi_t = 28.6 \times 10^4$ rad GHz^2. We consider a bright parabolic pump pulse of the form $P_{pump}(t) = P_{Pu\_Peak}[1\text{-}(t/T_{pump})^2]$, $|t| \le T_{pump}$, with a total temporal width of $T_{pump} = T_{probe} = 50$ ps. Note that for the design system, prior knowledge of the probe time duration is required to be covered by the pump pulse. In addition, the failure to fully cover the probe by the pump leads to a visible distortion on the mapped spectrum, specifically, the appearance of undesirable spectral oscillations. We choose a HNLF with an actual long-distance $L_{HNLF} = 1$ km, a nonlinear coefficient as high as $\gamma = 30$ W^{-1}.km^{-1}, a dispersion slope of 0.019 ps/nm^2/km, an attenuation coefficient of 1.3 dB/km at 1550 nm, and a zero-dispersion wavelength at $\lambda_0 = 1563$ nm [23]. The reason for choosing this type of HNLF is related to the derived condition (8), the more significant and reasonable values γ and L_{HNLF} take, the lower the P_{Pu_Peak} will be. We should mention that we use the same HNLF parameters for all subsequent results. From Eq. (8) and the declared parameters, the pump peak power should be $P_{Pu\_Peak} = 1.72$ W (32.36 dBm). Furthermore, to avoid the group velocity mismatch and dispersion, we set the probe and pump wavelengths to be symmetric and close enough to λ_0, $\lambda_{Pump} = 1554$ nm, and $\lambda_{Probe} = 1572$ nm. Finally, to confirm that self-phase modulation (SPM) does not play any role in our system, we put $P_{probe\_peak} = 6$ mW, where P_{probe_peak} is the peak power of the probe pulse, and to prove this supposition, we calculate the necessary distance L_{probe} where the SPM starts to have an important effect, as, $L_{HNLF} \ll L_{probe} = 1/(\gamma . P_{probe\_peak}) = 5.5$ km.

By neglecting Raman scattering, the third-order nonlinear self-steepening, and the higher terms of the second-order

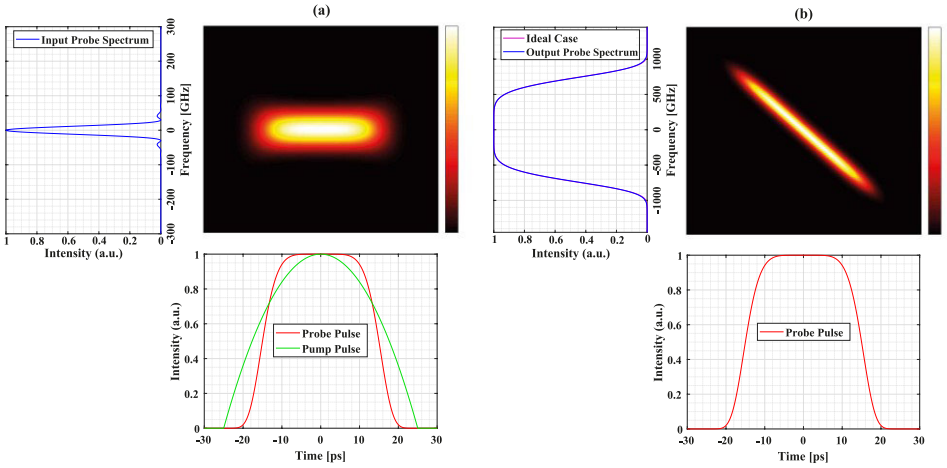

FIGURE 2. Far-field TFM for the case of a symmetric profile. (a) Input stage: the plot at the bottom shows the third order super-Gaussian probe and the bright parabolic pump in the time domain. The plot on the left shows the probe spectrum. The middle plot shows the spectrogram of the probe. (b) Output stage: the plot at the bottom shows the output probe in the time domain. The plot on the left shows the output probe spectrum after the mapping compared to the ideal case. The middle plot shows the spectrogram of the output probe.

dispersion, we performed the simulations based on the nonlinear Schrödinger equation solved numerically by the split-step Fourier method [22].

Fig. 2(a) and (b) show the input and output probe pulses before and after the XPM-based time-lens separately in both time and frequency domains, besides the two domains simultaneously. The plots at the bottom of the figures depict the temporal intensity profiles, and the plots at the left represent the spectral intensity. The middle images in the figures are the joint time-frequency intensity distribution (spectrogram), which gives information on the temporal location of the pulse's spectral components. The joint time-frequency intensity distribution of the pulses provides a better understanding of the physical processes of the XPM that determine the performance of the proposed system and its possible applications. The 2-D intensity distribution is displayed depending on the color brightness levels of the plot; the more lights on, the higher the intensity. The intensity distribution has been computed using a conventional spectrogram with a Hann time window of 10 ps duration. The result is compared with the ideal case where the input probe is mapped point by point directly to the frequency domain by scaling the time axis to a frequency axis supposing that $t = \omega/\varphi_t$, which is plotted in Fig. 2 (b) left (purple curve). The results displayed in the figures are in good agreement with our theoretical expectations. The output spectral intensity of the probe is identical to the temporal intensity profile of the input probe and matches perfectly with the ideal case. The results demonstrate the benefit of the XPM's intrinsic properties in providing high time resolution in such a manner that only a single dominant frequency term exists at a specific instant of time. It can be seen in the spectrogram, where the probe distributes its intensity in a linear way following the induced linear chirp. Furthermore, since the time-lens process manipulates the spectrum by distorting and broadening it, our system is not restricted by the output bandwidth, unlike other methods where the input bandwidth should be narrower than the system's bandwidth.

For deeper insight into the physical process, Fig. 3 shows the evolution of the spectrum along the HNLF. The variation of the temporal phase by the XPM effect exposes the pulse to a positive frequency chirp; the leading edge of the probe is shifted to lower frequencies, and the trailing edge to higher frequencies. Thus, new frequency components will be generated along the spectrum probe, and the spectrum will broaden when the nonlinear phase increases. Hence, the spectrum undergoes a significant broadening until it becomes a replica version of the input probe pulse.

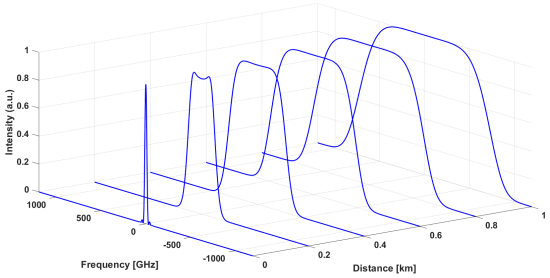

FIGURE 3. Evolution of the probe spectrum in the HNLF as a function of distance.

In order to provide a complete analysis of all possible cases, we study the case when P_{Pu_Peak} does not satisfy condition (8) [Fig. 4]. In particular, we violate the far-field criterion by making the amount of the linear chirp coefficient equal to the right-hand side terms in the inequality (3) (n = 1), $\varphi_t = 7.14 \times 10^4$ rad GHz^2, which corresponds to a P_{Pu_Peak} of 430.3 mW (26.33 dBm). Fig. 4 represents the

output stage, the bottom plot for the time representation, the left plot for the frequency representation, and the spectrogram of the resultant pulse at the system's output. Knowing that we maintain the same input probe pulse as in the previous case. In this case, the nonlinear effect of the XPM is not sufficiently strong to get an effective broadening of the pulse spectrum. It can be observed from the spectrogram that the output pulse energy is distributed over a wider frequency range at each instant of time. As a consequence, the output spectrum covers a narrower frequency range (∼600 GHz) compared to the previous case (∼2 THz) when the inequality (3) was verified. Additionally, the output spectrum exhibits visible distortions compared to the temporal profile, specifically the presence of undesirable spectral modulation in the flat-top region. These distortions come from the non-negligible quadratic phase term $\exp[-j(1/2\varphi_t)\sigma^2]$ in the integral of Eq. (2). These results can be interpreted by the fact that the input probe spectrum exhibits multiple secondary lobes, so the inequality (3) requires a notably larger linear chirp, corresponding to a larger P_{Pu_Peak}. There are two solutions to achieve TFM with this specific P_{Pu_Peak} value. The first is to impose a condition on the input total temporal width to be longer, which allows us to get a narrow input probe spectrum to fulfill the inequality (3). Secondly, an efficient way to overcome the described limitation of the far-field TFM method, without replacing the input probe pulse, is to use a linear dispersive medium to provide a spectral phase modulation with an opposite sign to the quadratic phase term $\exp[-j(1/2\varphi_t)\sigma^2]$, which means that the generated spectrum is no longer restricted by the far-field condition in the inequality (3). This approach is known as near-field TFM, which will be discussed in detail in the next section.

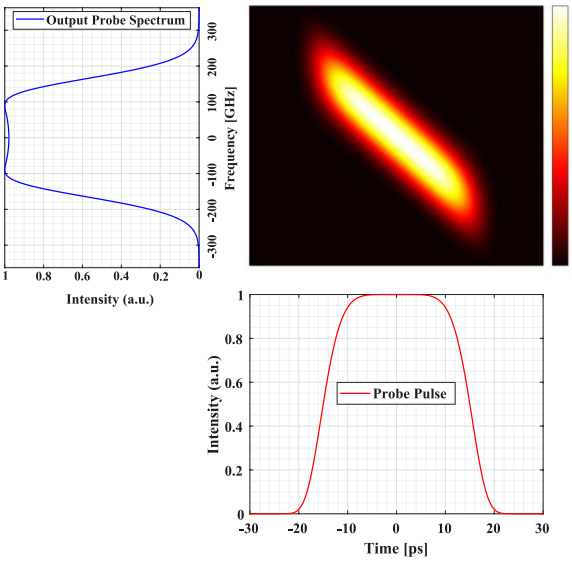

FIGURE 4. Results of the TFM when the pump peak power does not satisfy the necessary condition. Output stage: the plot at the bottom shows the output probe in the time domain. The plot on the left shows the distorted output probe spectrum after the mapping. The middle plot shows the spectrogram of the output probe.

We now focus our attention on system tunability, which can be achieved based on two strategies. The first one is to cover a longer duration by the pump, and we control the pump peak power depending on the input probe as long as $T_{pump} \geq T_{probe}$, which can be seen in Fig. 5, the first row (a). In our example, the pump covers a 55 ps time duration to convert input probes having different durations of 25, 35, 45, and 55 ps, equivalent to a total bandwidth of 426.7, 304.6, 237, and 193.6 GHz, respectively. The corresponding P_{Pu_Peak} for each of those durations is found to be 8.34, 4.25, 2.57, and 1.72 W, respectively. This strategy is more stable and easier to implement since the reconfigurability of the pump duration is no longer needed, but as can be seen, it requires a significant amount of energy in relation to short input probes. One could say that the shorter the probe, the more $\Delta\omega_{in}$ (the input bandwidth of the probe) increases, leading to a significant needed value of φ_t and, of course, according to condition (8), a significant amount of energy since T_{pump} is fixed.

The second strategy is that the total temporal width of the pump T_{pump} is tuned proportionally with the probe ($T_{pump} = T_{probe}$), as illustrated in Fig. 5 in the second row (b). For this time, the corresponding P_{Pu_Peak} is 1.72 W for all time durations. This result is quite surprising, indicating that more power is unnecessary to tune the system for different ranges of durations. Precisely, these results can be analyzed based on condition (8), which consists of two variables, T_{pump} and φ_t, that apparently vary in the same manner but with different signs. In fact, as the total temporal width T_{probe} increases, $\Delta\omega_{in}$ decreases as a reciprocal function, and since φ_t is related to the square of $\Delta\omega_{in}$, we could say that the variations of T_{pump} and φ_t compensate each other simply because they vary according to a quadratic function but with different signs. This reasoning is valid only if $T_{pump} = T_{probe}$. This strategy is more complicated compared to the first one since the reconfigurability of the pump duration is needed for each probe time duration, but as can be seen, it requires a low amount of energy. The assumption of the pump's reconfigurability can be met with state-of-the-art, and the easiest way is to use a programmable shaper such as the WaveShaper 4000S.

The two strategies provide the same results of the mapped spectrum regarding the shape and bandwidth, as shown in Fig. 5 in the third row (c), knowing that the bandwidth of the generated spectrum $\Delta\omega_{out}$ is determined by,

$$\Delta\omega_{out} = \varphi_t T_{probe} \tag{9}$$

This reasoning implies that for a certain value of $\Delta\omega_{out}$, the two strategies verify the same balance between T_{probe} and φ_t for any target probe duration due to condition (8), which gives the options for the proposed system implementation, taking into account the advantages and disadvantages discussed.

Now, we consider a non-symmetric profile (similar to a sawtooth pulse) with a 50 ps time duration as a probe pulse. The total bandwidth of this probe pulse was found to be 162 GHz, which gives $\varphi_t = 16.48 \times 10^4$ rad GHz^2 and $P_{Pu\_Peak} = 993.7$ mW (29.97 dBm). The bright parabolic

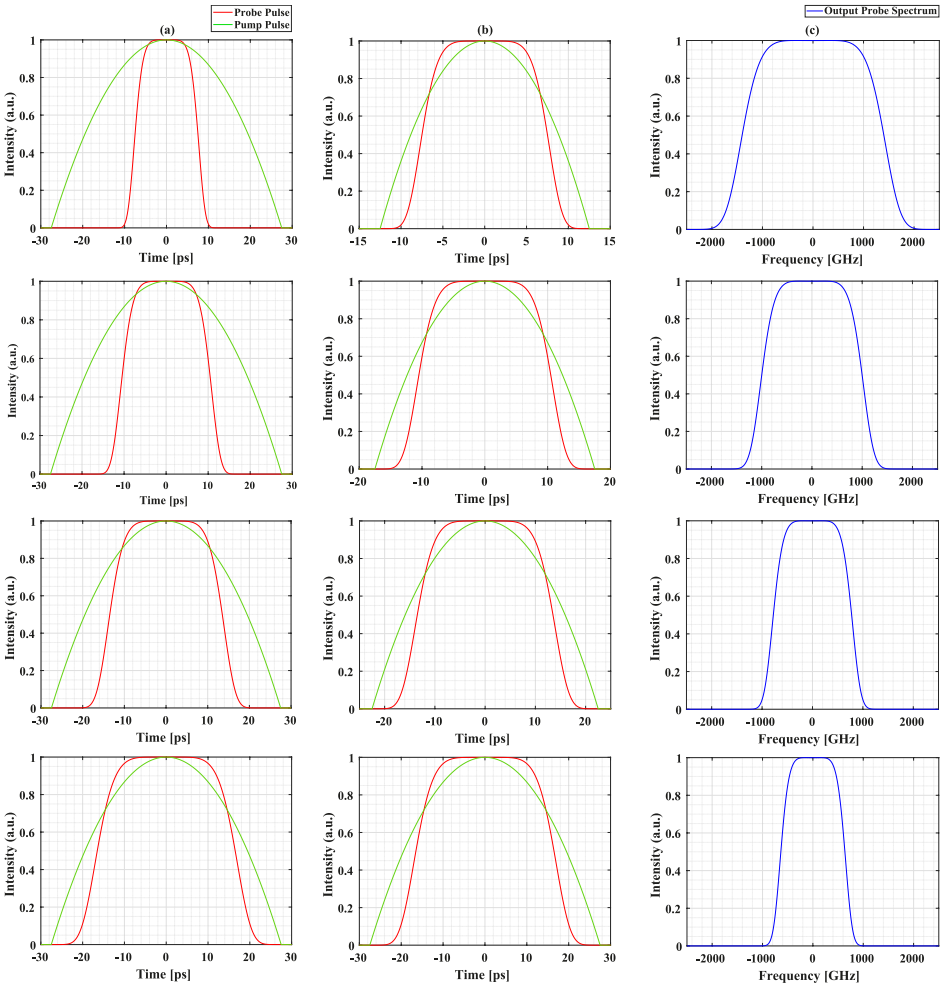

FIGURE 5. The system tunability using two strategies. (a) The pump duration is fixed, and the far-field TFM is performed by controlling the pump peak power according to the probe duration. (b) The pump duration is adjusted proportionally to the probe duration, and the pump peak power is fixed at a constant value for all durations. (c) The output probe spectrum after the mapping using the two strategies.

pump has the same total temporal width as the probe. Fig. 6(a) at the bottom represents the probe and the bright pump before propagating in the HNLF; at the left is the associated probe spectrum, and in the middle is the spectrogram of the input probe. For this case, the output spectrum (Fig. 6(b) left) is an inverted replica of the input temporal probe pulse compared to what should have been obtained (ideal case, purple curve). These results can be interpreted by the fact that the pump's induced chirp is positive over the central portion of the input probe pulse since the induced chirp of a bright parabolic profile is known to have a positive sign. We could say that the observation of TFM depends on the sign of the linear chirp coefficient in the case of non-symmetric profiles.

To overcome this limitation, we use the other class of parabolic pulses, known as dark parabolic pulses, defined as $P_{pump}(t) = P_{Pu\_Peak}[(t/T_{pump})^2]$, $|t| \leq T_{pump}$, which can offer the same linear chirp but with the opposite sign. The dark pulse has zero amplitude at its center and reaches maximum power toward the pulse edges. We reproduce the same simulation as in the previous case for the non-symmetric profile and observe the results in Fig. 7. The pump pulse verifies the required conditions, and the output probe's spectrum coincides with the input one's temporal profile. The fact that the spectrogram exhibits an inverse version of the previous one confirms that a different chirp sign is implemented. The average pump power of the dark pulse was 331.3 mW (25.2 dBm), which is relatively low (by half) compared to the bright pulse 662.6 mW (28.21 dBm) to induce the same chirp, as the average power of the bright and dark pulses is given by $(2/3)P_{Pu\_Peak}$ and $(1/3)P_{Pu\_Peak}$, respectively. We should mention that if we apply a dark parabolic pump to a symmetric profile, the results are the same as in the case of a bright parabolic pump since they provide the same chirp but with different signs.

To generalize these results in terms of the required average pump power of the bright/dark pumps and the target

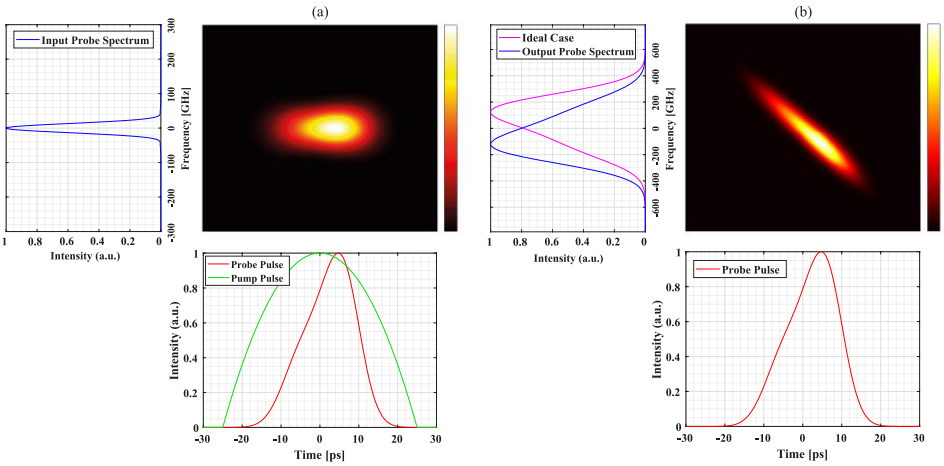

FIGURE 6. The case of a non-symmetric profile with bright parabolic pump. (a) Input stage: the plot at the bottom shows the sawtooth probe and the bright parabolic pump in the time domain. The plot on the left shows the probe spectrum. The middle plot shows the spectrogram of the probe. (b) Output stage: the plot at the bottom shows the output probe in the time domain. The plot on the left shows the output probe spectrum after the mapping (inverted replica of the ideal case). The middle plot shows the spectrogram of the output probe.

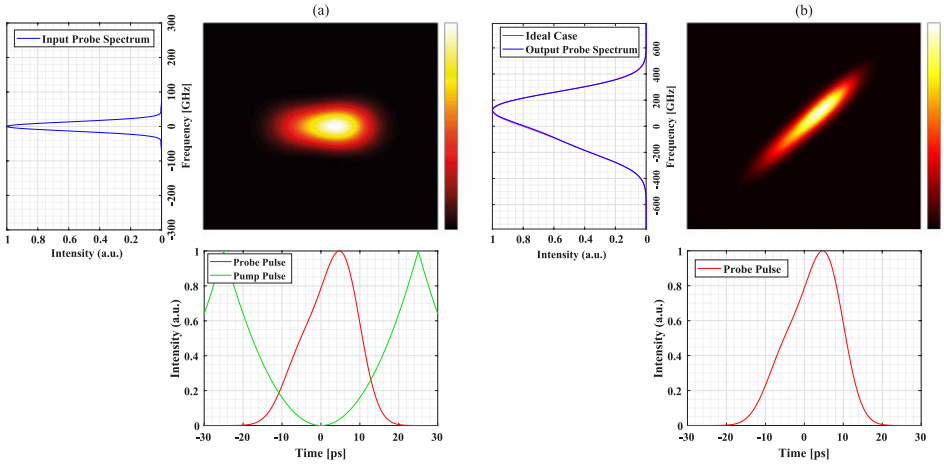

FIGURE 7. The case of a non-symmetric profile with dark parabolic pump. (a) Input stage: the plot at the bottom shows the sawtooth probe and the dark parabolic pump in the time domain. The plot on the left shows the probe spectrum. The middle plot shows the spectrogram of the probe. (b) Output stage: the plot at the bottom shows the output probe in the time domain. The plot on the left shows the output probe spectrum after the mapping (identical to the ideal case). The middle plot shows the spectrogram of the output probe.

probes with different shapes and durations, we follow the next steps,

- We generate three target probes with well-defined profiles: super-Gaussian, sawtooth, and triangular.
- Each profile is assigned a total temporal width ranging from $T_{probe} = 10$ to 100 ps.
- For each total temporal width, we calculate the total input bandwidth, the corresponding linear chirp coefficient by putting $n = 4$, and the required average pump power based on condition (8) for both the bright and dark parabolic pumps.
- The whole process is divided into two main categories: the first is to tune the total temporal width of the pump T_{pump} proportionally with the probe during the simulation, and the second is to fix the pump by putting $T_{pump} = 100$ ps.

Fig. 8 depicts the obtained results. To validate these results, the mapped spectrum has been verified compared to the ideal case for each profile during the simulation when T_{probe} ranged from 10 to 100 ps. For the first category ($T_{pump} = T_{probe}$), as already mentioned, the average pump power is constant for the entire temporal range for all profiles. The average pump power depends on the different input spectra of the target probes, which impose different conditions on φ_t. Also, as previously stated, using the dark pump significantly reduces the power by half compared to the bright one.

The average pump power using the bright pump takes the values 30.6, 28.17, and 29.88 dBm for the super-Gaussian, sawtooth, and triangular, respectively, and on the other hand, the average pump power using the dark pump takes the values 27.6, 25.16, and 26.87 dBm, respectively. For the second category ($T_{pump} \geq T_{probe}$), when T_{probe} takes a short duration compared to T_{pump}, the required average pump power takes unacceptable values due to the huge input bandwidth, which forces the chirp coefficient to take a significant value. The closer the duration of the probe is to the pump, the more the average pump power is acceptable, and we get closer to the first category.

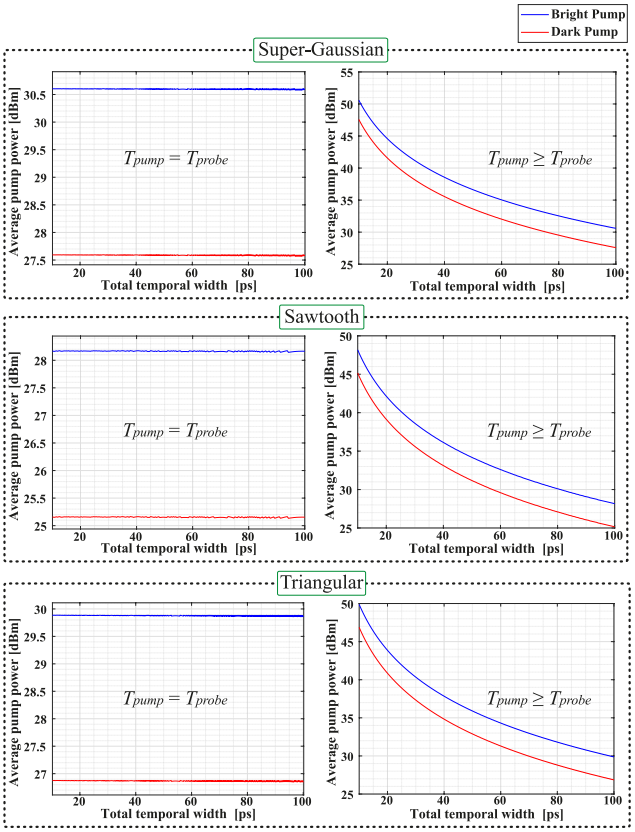

FIGURE 8. The average power of the bright/dark parabolic pumps as a function of the total temporal width of different target probe profiles.

B. NEAR-FIELD TIME-TO-FREQUENCY MAPPING

Until now, the TFM has been performed without any condition on the output spectral bandwidth. This section shows that a flat spectrum with a specific bandwidth can be generated without any condition on the input total temporal width.

In order to observe the limitation of the far field TFM method, assuming we have an unchirped third-order super-Gaussian profile with a time duration of $T_{probe} = 20$ ps (zero-to-zero full width of $\sim$ 533 GHz). The TFM system is designed to target an output bandwidth of 300 GHz. Once the output bandwidth is fixed, the linear chirp coefficient is obtained from the expression (9) and must satisfy $\varphi_t = 94.24 \times 10^3$ rad GHz^2. The used bright pump has a total

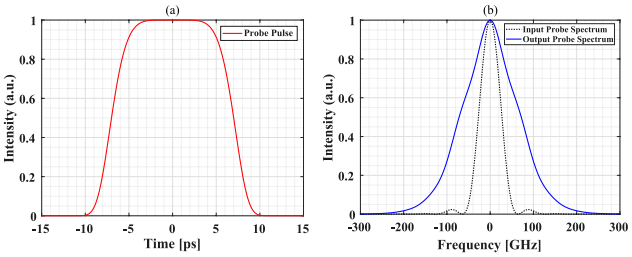

FIGURE 9. The limits of TFM in the far field regime. (a) The input probe pulse in the time domain with 20 ps temporal width. (b) Input and output probe spectrum.

temporal width of $T_{pump} = T_{probe} = 20$ ps, and the HNLF parameters are the same as in the previous section. Based on these parameters, the pump peak power is calculated and found to be $P_{Pu\_Peak} = 90.88$ mW (19.58 dBm). A numerical calculation was carried out and shown in Fig. 9. Our results show that the output spectrum undergoes a strong distortion due to the constraints of the far-field TFM method. In fact, the output bandwidth forces the linear chirp coefficient to take a specific value, which is not enough for the inequality (3) and results in a not fully satisfied value of the pump peak power. Knowing that the duration of the pulse probe restricts the input bandwidth since it is considered fixed. We could say that the far-field condition in inequality (3) limited the narrowband generation by the proposed scheme.

A practical solution to overcome this limitation is to simply propagate the probe in a dispersive medium before the XPM process. The spectral response of a dispersive medium can be modeled as a linear time-invariant system similar to a linear optical phase filter with a quadratic phase term of the form $\exp[-j(\beta_2 z/2)\omega^2]$, where β_2 is the group-velocity dispersion (GVD), and z is the propagation distance. We should mention that the constant phase factor β_0 and the average group delay β_1 are ignored in the following discussion since they are not responsible for pulse spreading over time. Also, the remaining higher-order dispersion terms are being ignored since we are dealing with narrow-bandwidth optical pulses in dielectric media. The dispersion regime in standard single-mode fibers (SMF) at λ_{Probe} is known to be anomalous (β_2 is less than zero), so the dispersive effect will provide a positive phase modulation of the form $\exp[j(\Phi_2/2)\omega^2]$, where Φ_2 is the second-order dispersion coefficient given as $\Phi_2 = \beta_2 z$. Thus, the new input spectrum $A_{in}(\omega)$' can be mathematically described by a multiplication of the input probe pulse $A_{in}(\omega)$ with the quadratic phase term of the dispersive medium (SMF). By associating this phase term with the input probe pulse in Eq. (2), the phase term $\exp[-j(1/2\varphi_t)\sigma^2]$ is canceled out as long as,

$$\varphi_t \Phi_2 = 1 \tag{10}$$

In this case, the generated spectrum is no longer restricted by the far-field condition in the inequality (3). In order to confirm this assumption, we reproduce the last simulation, noting that the temporal width of the pump must be changed to cover

a wider temporal range since the dispersion effect broadens the new probe, and hence, the pump peak power must also take a different value. First, we calculate the second-order dispersion coefficient by Eq. (10), $\Phi_2 = 10.61$ ps^2. This value can be obtained using Corning SMF-28e with a dispersion parameter of D $\leq$ 18 ps /(nm.km), dispersion slope of $S_0 \leq$ 0.089 ps/(nm^2.km) at 1550 nm, and zero dispersion wavelength of 1302 nm $\leq \lambda_0 \leq$ 1322 nm. The GVD at λ_{Probe} has been calculated and found to be $\beta_{2,1572\text{nm}} = -23.74$ ps^2/km, indicating that to reach the desirable value of Φ_2, we must use a fiber of 447 m long. Secondly, we calculate the new time duration after the broadened probe, $T_{probe} \approx 50$ ps. Finally, we chose the corresponding time duration of the pump, $T_{pump} = 50$ ps. In this case, the pump peak power must be $P_{Pu\_Peak} = 568$ mW (27.54 dBm). The results are depicted in Fig. 10. By performing the proposed solution of the near-field TFM, this time, the output probe spectrum closely resembles the initial input probe pulse and has the targeted frequency bandwidth of 300 GHz. In this way, we can generate any narrowband spectrum with a specific shape and bandwidth via two factors, the amount of dispersion and the corresponding power according to condition (8).

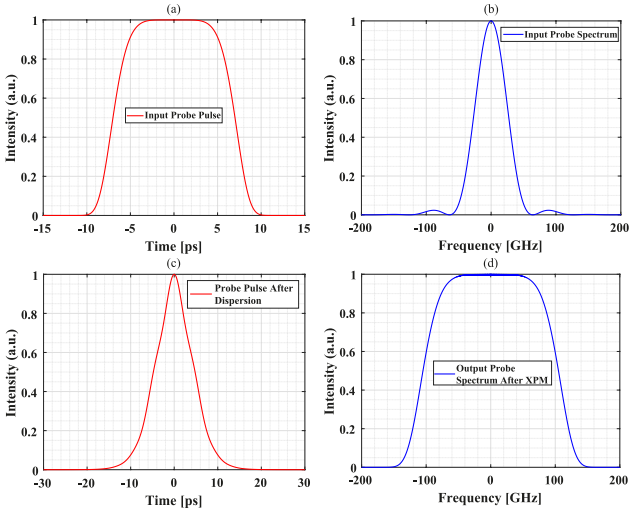

FIGURE 10. Near-field TFM. (a) The input probe pulse in the time domain with 20 ps temporal width. (b) The input probe spectrum with ∼533 GHz bandwidth. (c) The probe pulse after the dispersion effect with ∼50 ps temporal width. (d) The output probe spectrum after the XPM with third order super-Gaussian profile and 300 GHz bandwidth.

To determine the minimum bandwidth of the generated probe spectrum, equation (9) indicates that there are three cases to study,

First case: T_{probe} is fixed (the most common scenario). In this case, when we target a lower $\Delta\omega_{out}$, φ_t should take a lower value and force P_{Pu_Peak} to be low according to condition (8). By going forward, we arrive at the point where P_{Pu_Peak} cannot induce the nonlinear effect into the HNLF, which determines the minimum bandwidth of the generated probe spectrum. We could say that this limit is directly related to the physical properties of the HNLF. It should be noted that when φ_t takes a lower value, Φ_2 should be high enough to achieve the dispersion-XPM balance according to equation 10.

Second case: φ_t is fixed. In this case, if we aim for a lower $\Delta\omega_{out}$, T_{probe} should take shorter durations. Going further, we reach the point where T_{probe} enters the femtosecond regime, which requires specific light sources or compression techniques. On the other hand, since we are dealing with pulses in the femtosecond regime (large-bandwidth optical pulses), we run the risk of generating higher-order dispersion terms in the dielectric medium (specifically the optical fiber used at the input for near-field TFM). We can say that the minimum generated bandwidth depends on the minimum reasonable duration of T_{probe}.

Third case: minimum values of T_{probe} and φ_t. This case could provide the lowest possible bandwidth when we reach the limit of the previous two cases.

This reasoning is valid only in near-field TFM, where T_{probe} and φ_t are completely independent, unlike in far-field TFM, where φ_t is linked to the input bandwidth of the probe.

C. DISCUSSION OF POTENTIAL APPLICATIONS

In order to provide more insight into the developed approach, a discussion of its potential application in a variety of fields is necessary. Highly flat and narrow optical frequency combs (OFC) generation is needed for various applications, including coherent WDM transmission, high modulation formats beyond 16-QAM, and local oscillation [24], [25], [26]. TFM has already been exploited to generate Flat-top OFC with 27 comb lines, a 3 dB flatness, and a 10-GHz interval using EO-PM driven by sinusoidal signals [27]. The bandwidth of the EO-PM limits this last work, and the RF linewidth of the individual modes has not been discussed. D. Hillerkuss et al [28] propose a spectral slicing technique based on SPM using a Waveshaper with 10 GHz channel spacing to obtain 325 consecutive equidistant comb lines with 4 THz bandwidth and low phase noise of 1 kHz linewidth to obtain 325 with 4 THz bandwidth. A closer analysis of our obtained flat spectrum reveals that TFM could be helpful for high-quality OFC by the slicing technique with significant advantages such as:

- Energy conservation due to the use of phase-only temporal filtering allows us to overcome the critical limitations of direct Fourier domain techniques.
- Our approach requires an input temporal shape with a well-defined profile to obtain the target spectrum, compared to the approach in [28], where double stages are needed to form a continuous broad output spectrum.
- Additionally, our method offers the tunability to control the output spectral bandwidth, whether wide or narrow.

Furthermore, TFM can be used directly as a measurement method for ultrashort optical pulses [29] by extracting the spectral features of the mapped pulse with a spectrum analyzer and transferring them to the temporal domain. Unlike other methods, our method offers a fast, high-resolution, noniterative, and accurate temporal waveform measurement,

especially suited for the measurement range from sub-femtosecond to about a nanosecond duration.

Other applications have been reported based on TFM, including photonic analog-to-digital conversion, optical time division multiplexed to dense wavelength division multiplexed conversion, the enhancement of radiofrequency photonic filters, and as a method for distortion-free optical transmission for any kind of linear perturbation such as higher-order dispersion, time jitter, polarization-mode dispersion, and time-varying dispersion [30], [31], [32], [33].

IV. CONCLUSION

In conclusion, starting from the far-field spectral Fraunhofer regime and parabolic XPM, we deduced an equation linking the pump peak power with the linear chirp coefficient and the prerequisites of the XPM process to realize a developed approach for tunable all-optical time-to-frequency mapping. Numerical simulation confirms the validity of the derived condition, and a pure mapping was obtained by a single all-optical time lens as long as the far-field spectral Fraunhofer regime is respected. The developed approach can be applied to any probe pulse profile since the derived condition is related to the input spectral bandwidth of the probe and not its profile. In order to optimize the results, the type of HNLF was carefully chosen to relax the pump peak power, and the probe and pump wavelengths were set to be symmetric and close enough to zero dispersion wavelength to eliminate all possible linear degradation, such as dispersion and walk-off effects.

Additionally, we have demonstrated that system tunability can be achieved through two strategies. The first is by fixing the duration of the pump and modifying the power according to the duration of the probe. This strategy is stable and simple to implement, but it requires high energy values when targeting short probe durations. The second is by fixing the power and tuning the duration of the pump proportionally to the probe. This last strategy leads us to conclude that, in order to convert input probes with different profiles and durations, more power is unnecessary as long as the duration of the pump is tuned proportionally to the probe. The second strategy is solid in terms of power but requires reconfigurable techniques to adjust the duration of the pump.

Further, we proposed a family of bright and dark parabolic pulses that could be employed depending on the symmetric and non-symmetric probe pulses. We have shown that the observation of TFM depends on the sign of the linear chirp coefficient in the case of non-symmetric profiles, and the use of dark parabolic pulses is considered as a solution to avoid the inverted mapped replica of the input temporal probe pulse. In fact, the bright and dark parabolic pulses provide the same chirp but with different signs. The main difference is that the average pump power of the dark pulse is relatively low (by half) compared to the bright pulse to induce the same chirp. This conclusion allows us to use the dark parabolic pulses in symmetric and asymmetric cases, unlike the bright ones, but with more complicated strategies to generate them.

We have also studied the case when the output spectral bandwidth is restricted by the limits of the far-field TFM, where a single all-optical time lens cannot generate a narrow bandwidth. A solution based on near-field TFM has been proposed by employing a dispersive medium in the system to create a dispersion-XPM balance, and the desired spectrum has been successfully generated since it's no longer restricted by the far-field condition. However, even when we deal with near-field TFM, the derivative condition is necessary and plays an important role in achieving the balance of dispersion-XPM.

Finally, we discussed some potential applications in various fields in order to increase the scope of the approach, mainly in the generation of optical frequency combs and the characterization of ultrashort pulses.

REFERENCES

[1] C. Schnébelin, J. Azaña, and H. G. D. Chatellus, "Programmable broadband optical field spectral shaping with megahertz resolution using a simple frequency shifting loop," *Nature Commun.*, vol. 10, no. 1, p. 4654, Oct. 2019.

[2] A. Bahabad, M. M. Murnane, and H. C. Kapteyn, "Manipulating nonlinear optical processes with accelerating light beams," *Phys. Rev. A, Gen. Phys.*, vol. 84, no. 3, Sep. 2011, Art. no. 033819.

[3] M. Konsens and A. Bahabad, "Time-to-frequency mapping of optical pulses using accelerating quasi-phase-matching," *Phys. Rev. A, Gen. Phys.*, vol. 93, no. 2, Feb. 2016, Art. no. 023823.

[4] D. Wang, L. Huo, Q. Wang, X. Chen, and C. Lou, "Time-to-frequency conversion based on nonlinear pulse shaping," in *Proc. Conf. Lasers Electro-Opt. (CLEO)*, Jun. 2014, pp. 1–2.

[5] J. Azaña, N. K. Berger, B. Levit, and B. Fischer, "Spectral Fraunhofer regime: Time-to-frequency conversion by the action of a single time lens on an optical pulse," *Appl. Opt.*, vol. 43, no. 2, pp. 483–490, 2004.

[6] N. K. Berger, B. Levit, S. Atkins, and B. Fischer, "Time-lens-based spectral analysis of optical pulses by electrooptic phase modulation," *Electron. Lett.*, vol. 36, no. 19, pp. 1644–1646, Sep. 2000.

[7] J. P. Limpert, T. Schreiber, T. Clausnitzer, K. Zöllner, H. J. Fuchs, E. B. Kley, H. Zellmer, and A. Tünnermann, "High-power femtosecond Yb-doped fiber amplifier," *Opt. Exp.*, vol. 10, no. 14, pp. 628–638 2002.

[8] C. Finot, J. M. Dudley, B. Kibler, D. J. Richardson, and G. Millot, "Optical parabolic pulse generation and applications," *IEEE J. Quantum Electron.*, vol. 45, no. 11, pp. 1482–1489, Nov. 2009.

[9] P. Dupriez, C. Finot, A. Malinowski, J. K. Sahu, J. Nilsson, D. J. Richardson, K. G. Wilcox, H. D. Foreman, and A. C. Tropper, "High-power, high repetition rate picosecond and femtosecond sources based on Yb-doped fiber amplification of VECSELs," *Opt. Exp.*, vol. 14, no. 21, pp. 9611–9616, 2006.

[10] F. Parmigiani, C. Finot, K. Mukasa, M. Ibsen, M. A. F. Roelens, P. Petropoulos, and D. J. Richardson, "Ultra-flat SPM-broadened spectra in a highly nonlinear fiber using parabolic pulses formed in a fiber Bragg grating," *Opt. Exp.*, vol. 14, no. 17, pp. 7617–7622, 2006.

[11] T. Hirooka, M. Nakazawa, and K. Okamoto, "Bright and dark 40 GHz parabolic pulse generation using a picosecond optical pulse train and an arrayed waveguide grating," *Opt. Lett.*, vol. 33, no. 10, pp. 1102–1104, 2008.

[12] J. Huh and J. Azaña, "Generation of high-quality parabolic pulses with optimized duration and energy by use of dispersive frequency-to-time mapping," *Opt. Exp.*, vol. 23, no. 21, pp. 27751–27762, 2015.

[13] S. Pitois, C. Finot, J. Fatome, B. Sinardet, and G. Millot, "Generation of 20-GHz picosecond pulse trains in the normal and anomalous dispersion regimes of optical fibers," *Opt. Commun.*, vol. 260, no. 1, pp. 301–306, Apr. 2006.

[14] A. Halassi, Y. Driouche, R. Hamdi, and B.-E. Benkelfat, "Generalized temporal synthesis method for a birefringent laser pulse shaper," *J. Opt. Soc. Amer. A, Opt. Image Sci.*, vol. 37, no. 11, p. C15, 2020.

[15] F. Liu, S. Huang, S. Si, G. Zhao, K. Liu, and S. Zhang, "Generation of picosecond pulses with variable temporal profiles and linear polarization by coherent pulse stacking in a birefringent crystal shaper," *Opt. Exp.*, vol. 27, no. 2, pp. 1467–1478, 2019.

[16] R. Salem, M. A. Foster, and A. L. Gaeta, "Application of space-time duality to ultrahigh-speed optical signal processing," *Adv. Opt. Photon.*, vol. 5, no. 3, pp. 274–317, Sep. 2013.
[17] F. Parmigiani, P. Petropoulos, M. Ibsen, and D. J. Richardson, "Pulse retiming based on XPM using parabolic pulses formed in a fiber Bragg grating," *IEEE Photon. Technol. Lett.*, vol. 18, no. 7, pp. 829–831, Apr. 1, 2006.
[18] T. T. Ng, F. Parmigiani, M. Ibsen, Z. Zhang, P. Petropoulos, and D. J. Richardson, "Compensation of linear distortions by using XPM with parabolic pulses as a time lens," *IEEE Photon. Technol. Lett.*, vol. 20, no. 13, pp. 1097–1099, Jul. 1, 2008.
[19] T. Hirooka and M. Nakazawa, "All-optical 40-GHz time-domain Fourier transformation using XPM with a dark parabolic pulse," *IEEE Photon. Technol. Lett.*, vol. 20, no. 22, pp. 1869–1871, Nov. 15, 2008.
[20] A. Zohrabyan, A. A. Kutuzian, V. J. Ninoyan, and L. K. Mouradian, "Spectral compression of picosecond pulses by means of cross-phase modulation," *AIP Conf. Proc.*, vol. 406, no. 1, pp. 395–401, Apr. 1997.
[21] L. K. Mouradian, F. Louradour, V. Messager, A. Barthelemy, and C. Froehly, "Spectro-temporal imaging of femtosecond events," *IEEE J. Quantum Electron.*, vol. 36, no. 7, pp. 795–801, Jul. 2000.
[22] G. P. Agrawal, *Nonlinear Fiber Optics*. New York, NY, USA: Academic, 2007.
[23] T. Nakanishi, M. Hirano, T. Okuno, and M. Onishi, "Silica-based highly nonlinear fiber with γ = 30/W/km and its FWM-based conversion efficiency," in *Proc. Opt. Fiber Commun. Conf. Nat. Fiber Optic Eng. Conf.*, 2006, p. 3.
[24] P. Marin-Palomo, J. N. Kemal, P. Trocha, S. Wolf, K. Merghem, F. Lelarge, A. Ramdane, W. Freude, S. Randel, and C. Koos, "Comb-based WDM transmission at 10 Tbit/s using a DC-driven quantum-dash mode-locked laser diode," *Opt. Exp.*, vol. 27, no. 22, pp. 31110–31129, 2019.
[25] J. N. Kemal, P. Marin-Palomo, V. Panapakkam, P. Trocha, S. Wolf, K. Merghem, F. Lelarge, A. Ramdane, S. Randel, W. Freude, and C. Koos, "Coherent WDM transmission using quantum-dash mode-locked laser diodes as multi-wavelength source and local oscillator," *Opt. Exp.*, vol. 27, pp. 31164–31175, Oct. 2019.
[26] J. N. Kemal, P. Marin-Palomo, K. Merghem, G. Aubin, F. Lelarge, A. Ramdane, S. Randel, W. Freude, and C. Koos, "32QAM WDM transmission at 12 Tbit/s using a quantum-dash mode-locked laser diode (QD-MLLD) with external-cavity feedback," *Opt. Exp.*, vol. 28, no. 16, pp. 23594–23608, 2020.
[27] J. Yan, Y. Peng, X. Yao, M. Bai, and Z. Zheng, "Generation of optical frequency combs based on time-to-frequency conversion," *IET Optoelectron.*, vol. 8, no. 3, pp. 149–153, Jun. 2014.
[28] D. Hillerkuss, T. Schellinger, M. Jordan, C. Weimann, F. Parmigiani, B. Resan, K. Weingarten, S. Ben-Ezra, B. Nebendahl, C. Koos, W. Freude, and J. Leuthold, "High-quality optical frequency comb by spectral slicing of spectra broadened by SPM," *IEEE Photon. J.*, vol. 5, no. 5, Oct. 2013, Art. no. 7201011.
[29] Z. Qiao, X. Pan, X. Wang, T. Huang, P. Zhang, W. Fan, X. Li, and Z. Lin, "Characterization of ultrashort pulses by time-frequency conversion and temporal magnification based on four-wave mixing at 1 μm," *Appl. Opt.*, vol. 56, no. 8, pp. 2294–2300, 2017.
[30] H. Chi, Q. Zhang, S. Yang, B. Yang, Y. Zhai, and J. Ou, "Photonic analog-to-digital conversion based on time-to-frequency mapping," *Opt. Commun.*, vol. 502, Jan. 2022, Art. no. 127440.
[31] E. Palushani, H. C. H. Mulvad, M. Galili, H. Hu, L. K. Oxenlowe, A. T. Clausen, and P. Jeppesen, "OTDM-to-WDM conversion based on time-to-frequency mapping by time-domain optical Fourier transformation," *IEEE J. Sel. Topics Quantum Electron.*, vol. 18, no. 2, pp. 681–688, Mar. 2012.
[32] M.-H. Song, "Sidelobe suppression enhancement of radiofrequency photonic filters via time-to-frequency mapping," *J. Opt. Soc. Korea*, vol. 18, no. 5, pp. 449–452, Oct. 2014.
[33] T. Hirooka and M. Nakazawa, "Optical adaptive equalization of high-speed signals using time-domain optical Fourier transformation," *J. Lightw. Technol.*, vol. 24, no. 7, pp. 2530–2540, Jul. 2006.

YOUCEF DRIOUCHE received the master's and Ph.D. degrees in telecommunication systems from Université 08 Mai 1945 Guelma, Algeria, in 2018 and 2022, respectively. He is currently a Postdoctoral Researcher with the SAMOVAR Laboratory, Télécom SudParis, Institut Polytechnique de Paris, France. His current research interests include optical signal processing, nonlinear optics, optoelectronic systems, optical frequency combs for optical transmission, and photonic reservoir computing.

BADR-EDDINE BENKELFAT (Senior Member, IEEE) received the master's and Ph.D. degrees in optics and signal processing from the University of Franche-Comté, Besançon, France, in 1981 and 1984, respectively. In 1990, he joined the Institut Mines-Telecom, Telecom SudParis (formerly called INT), as an Associate Professor, and founded the Optics and Photonics Group. He is currently a Professor with the Electronics and Physics Department, INT. His current research interests include optoelectronic systems for data processing and optical devices for high-speed optical fiber communications.